Periodica Polytechnica Mechanical Engineering, 70(2), pp. 126–139, 2026

Study of MHD Flow of a Radiating Williamson Fluid Past a Non-linear Stretching Sheet

Sonam Garg[1], Rajendra Singh Yadav[1*]

[1] Department of Mathematics, Faculty of Science, University of Rajasthan, JLN Marg, 302004 Jaipur, Rajasthan, India
[*] Corresponding author, e-mail: rajendrauor@gmail.com

Received: 30 October 2024, Accepted: 21 March 2026, Published online: 09 April 2026

Abstract

This work examines the influence of a heat source/sink and dissipation on the MHD laminar flow of Williamson fluid over a nonlinear elastic sheet in a porous medium. The effects of non-linear radiation and Joule heating are also considered. The fluid's conductivity and viscosity are assumed to vary with temperature, enabling the study of heat and mass transfer phenomena. Suitable similarity variables are employed to transfer the resultant system of PDEs into a system of non-linear ODEs. The system is numerically solved utilizing the shooting approach in combination with the 4th-order Runge-Kutta method in MATLAB. The findings are validated through comparison with prior research, demonstrating a high level of agreement. The influence of various flow parameters on heat distribution and the flow field is analyzed and illustrated through diagrams. Additionally, the friction coefficient and Nusselt number are computed numerically for a range of selected parameters and presented in tables. Key findings reveal that the velocity profile decreases with an increase in the viscosity parameter, while temperature rises with a higher viscosity parameter. Moreover, the Nusselt number decreases with an increase in the Williamson, viscosity, and Eckert parameters, while it increased with the suction parameter. The findings may have significant applications in various industrial and scientific fields, particularly in paints and coating, oil drilling, and blood circulation.

Keywords

MHD flow, Joule heating, suction/blowing, viscous dissipation, porous medium

1 Introduction

The study of boundary layer flow of Williamson fluid over a stretching sheet is significant due to the importance of flow and heat transmission phenomena in manufacturing processes, contemporary technology, and industries. Applications include filtration techniques, paper manufacturing, steam generation, reactor fluidization, condensation processes, crystal growth, and metal spinning [1]. Sakiadis [2] was the first to propose the concept of boundary layer flow over a moving plate. Gupta and Gupta [3] expanded this concept by incorporating a stretching surface with suction/blowing. They observed that an increase in suction reduces the extent layer thickness, while the opposite is true for blowing. Patel and Patel [4] focused their research on fluid flow via a nonlinear stretching sheet, considering various effects such as mixed convection and porosity. In this research, the Homotopy Analysis Method has been utilized to perform numerical simulations. Choudhary et al. [5] analyzed the flow of a radiative tetra-hybrid nanofluid over a stretching surface within a porous medium. Jat et al. [6] investigated entropy generation in couple stress fluid flow over a stretching channel.

The theory of fluid flow in porous media plays a crucial role in research due to its wide applications across multiple fields of engineering and applied science, especially in purification systems, oil and gas recovery, catalysts, heat exchangers, mechanics, beverage processing, and rock formations. Porosity is a key factor in determining how solids physically interact with fluids in various technical applications [7]. Additionally, it has many uses in technologies like inkjet printing [8] and nuclear waste disposal [9]. Recently, the role of porous media on fluid flows under various conditions has been analyzed by many researchers [10–14]. They found that the porosity factor reduces flow velocity while having the opposite effect on heat transfer.

As we know, magnetohydrodynamics (MHD) has wide applications in medicine and engineering, particularly

Cite this article as: Garg, S., Yadav, R. S. "Study of MHD Flow of a Radiating Williamson Fluid Past a Non-linear Stretching Sheet", Periodica Polytechnica Mechanical Engineering, 70(2), pp. 126–139, 2026. https://doi.org/10.3311/PPme.38701

in tumor treatment, cell separation, blood flow, MHD pumps, solar physics, power generation, and tissue temperature regulation, making it a significant area of research [15]. MHD uses magnetic effects to study fluid dynamics. The mass and heat transmission in the extent layer flow over different geometries can be influenced by an applied magnetic field. The concept of magnetohydrodynamics was originally proposed by Alfvén [16]. Kolesnichenko [17] examined the structure of the MHD model for emulating turbulent motions. Later, Sharma et al. [18] studied the response of MHD flow in non-Newtonian fluids over a stretching sheet, considering the effects of Soret-Dufour, and slip conditions. They employed the Casson fluid model to describe the fluid's rheology. The outcomes revealed a significant reduction in velocity with an increase in the magnetic field. Additionally, the temperature increased with higher Dufour and Soret numbers. Recently, Tanwar et al. [19] analyzed the MHD flow of Williamson fluid under the influence of Soret-Dufour and found that the magnetic field reduced the flow.

In many systems, both suction and blowing are used in tandem to control fluid flow. For example, in HVAC systems, air is sucked in, cooled or heated, and then blown out. Suction is also used in medical systems to remove bodily fluids or other substances during surgeries. Conversely, blowing is applied in connecting reactor parts, cooling aircraft, and reducing drag [20]. Jyothi and Kudenatti [21] examined the influence of viscosity on the two-dimensional flow of fluid with suction/blowing in the context of a permeable wedge. They found that the suction parameter reduced both velocity and temperature, while the blowing parameter had the opposite effect. Jangid et al. [22] analyzed the impact of radiation on the hydromagnetic flow of Williamson fluid over an exponentially stretching sheet with suction/blowing and found an inverse relationship between the suction parameter and the temperature profile.

Non-Newtonian fluids have garnered significant attention from researchers due to their broad applications in various industrial and scientific fields, particularly in paints and coatings, oil drilling, blood circulation, and the formulation of beauty products. The most common type of non-Newtonian fluid is pseudoplastic fluid [23]. The Williamson fluid model describes the behavior of pseudoplastic fluids. Williamson [24] made a key contribution by explaining pseudoplastic substances and introducing a model for non-Newtonian fluids. Saleem and Hussain [25] investigated the role of electromagnetic forces on Williamson fluid flow along an exponentially elastic sheet, using the BVP4C approximation technique to obtain numerical solutions. Zafar et al. [26] explored key mechanisms of Williamson fluid motion over an elastic lubricant sheet and found that the Williamson parameters contribute to reducing the thickness of the extent layer. Jain et al. [27] numerically analyzed the behavior of Williamson nanofluid flowing through a permeable surface under mixed convection. Similarly, Choudhary et al. [28] investigated MHD Williamson fluid flow past a continuously moving thin needle and discussed the influence of Soret-Dufour effects on transport characteristics.

As we know, fluid properties such as viscosity and conductivity are typically assumed to be constant in most scientific literature [29, 30]. However, temperature-dependent fluid properties are preferred in many applications due to their wide relevance across various industries and scientific fields. Some of these applications include extrusion processes, food processing, blood flow, heat transfer, wire coating, chemical and polymer processing. Gosty et al. [31] and Imtiaz et al. [32] explored MHD flow through various layers with temperature-dependent fluid characteristics.

The concept of dissipation is significant due to its extensive applications in geophysical flows and various industrial processes [33]. Similarly, the influence of Joule heating is important because of its numerous applications in electrothermal flows, microfluidic channels, aerospace, and chemical engineering, particularly in cooling reactors [34]. Sadia et al. [35] investigated the influence of dissipation and heating on viscoelastic fluid over a rotating surface using the BVP4C technique. Ahmed et al. [36] analyzed the flow of a Carreau-Yasuda model through a wavy channel under the influence of dissipation and heating. They found that the Weissenberg number increased the flow near the lower part of the channel.

The occurrence of heat generation and absorption is a fascinating topic that has captivated many researchers due to its applications in various natural and industrial procedures, such as nuclear reactors, thermal power plants, vehicles, rocket engines, and dissociating liquids [37]. It affects the temperature distribution in fluid flows. Barman [38] analyzed the impact of a heat source on nanofluid flow over a vertical channel in a porous medium. They observed that the heat transfer rate decreased in the presence of a heat source. Previous literature [39, 40] has discussed the influence of heat generation/absorption on fluid flow through various types of geometries using different numerical techniques.

Moreover, the role of radiation in the fluid's heat transfer becomes particularly noticeable at elevated temperatures. It is well known that, in several non-isothermal conditions, the influence of radiation is crucial [41]. Additionally, in engines or industrial furnaces, radiation contributes to heat transfer between hot gases and chamber walls. Radiation can be a significant mechanism for cooling, especially in high-performance or compact electronic systems where other cooling methods may be less effective. Recently, the heat transport caused by the impact of radiation on the flow of non-Newtonian and nanofluids through various types of geometries has been discussed by numerous authors [42–45]. These studies found that temperature has a direct relationship with the radiation parameter.

The existing research reveals that although the effect of radiation on the flow of non-Newtonian fluid over stretching surfaces has been widely studied, several physical mechanisms have not yet been examined simultaneously. In particular, limited research has focused on Williamson fluid flow through a non-linear stretching sheet in a porous medium while considering the impacts of heat sources/sinks, dissipation, magnetic fields, variable conductivity and viscosity, non-linear thermal radiation, and Joule heating. Therefore, addressing this gap is the aim of this study.

The current work extends the analysis of Megahed [46] by incorporating porosity effects, Joule heating, magnetic fields, heat sources/sinks, suction/blowing, and dissipation, which is an innovative aspect of the study. These additional physical mechanisms provide a wide range of experimental applications in technology, biomedicine, and other chemical products. The solutions of this work are calculated using the shooting approach in combination with the 4th-order Runge-Kutta method.

2 Mathematical formulation

2.1 Physical configuration

The present problem deals with the steady, 2-D MHD flow of an incompressible Williamson fluid through a non-linearly stretching porous sheet. A coordinate system is selected such that the x-axis is taken along the sheet while the y-axis is perpendicular to it. The sheet stretches with a velocity

$$U_w(x) = ax^m$$

where $a > 0$ is the stretching parameter.

A spatially varying magnetic field is imposed perpendicular to the flow axis (x-axis) and is given by

$$B(x) = B_0 x^{\left(\frac{m-1}{2}\right)}$$

where B_0 indicates the strength of the magnetic field.

The physical configuration of the problem is shown in Fig. 1.

2.2 Assumptions

To simplify the physical problem, the following assumptions are considered:

1. The fluid flow is considered to be steady, 2-D, and laminar.
2. The working fluid behaves as an incompressible Williamson fluid.
3. The sheet is permeable and non-linearly stretched.
4. The fluid is electromagnetically conductive.
5. The flow is assumed to occur at a low Reynolds number, where viscous forces dominate the inertial forces, making the boundary layer formulation appropriate.
6. The thermal conductivity (k) and viscosity (μ) of the fluid are assumed to vary linearly and exponentially with temperature [47], respectively as

$$k(T) = k_\infty(1+\epsilon\theta), \quad \mu(T) = \mu_\infty e^{-\zeta\theta}.$$

7. The magnetic Reynolds number is sufficiently small; therefore, the propelled magnetic field and the Hall impact is disregard [48].

2.3 Governing equations

To conceptualize this type of flux model, the modelling equations are illustrated as follows [46, 49, 50]:

$$\frac{\partial u}{\partial x} + \frac{\partial v}{\partial y} = 0 \tag{1}$$

$$u\frac{\partial u}{\partial x} + v\frac{\partial u}{\partial y} = \frac{1}{\rho_\infty}\frac{\partial}{\partial y}\left(\mu(T)\frac{\partial u}{\partial y} + \mu(T)\frac{\Gamma}{\sqrt{2}}\left(\frac{\partial u}{\partial y}\right)^2\right) - \frac{\mu(T)u}{\rho_\infty K} - \frac{\sigma B^2 u}{\rho_\infty} \tag{2}$$

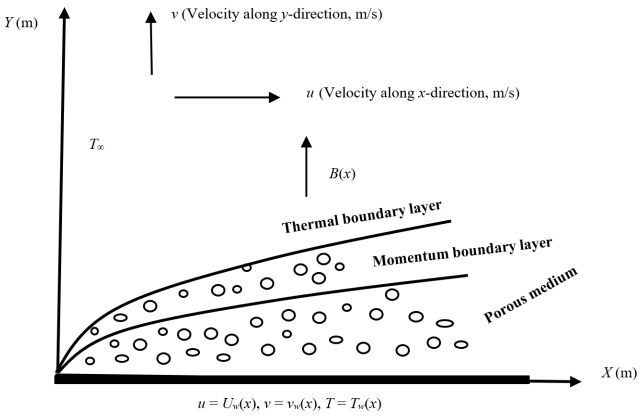


Fig. 1 Physical structure of fluid flow in porous medium

$$u\frac{\partial T}{\partial x}+v\frac{\partial T}{\partial y}=\frac{1}{\rho_\infty c_p}\begin{bmatrix}\frac{\partial}{\partial y}\left(k\left(T\right)\frac{\partial T}{\partial y}\right)-\frac{\partial q_r}{\partial y}\\+\mu\left(T\right)\left(1+\frac{\Gamma}{\sqrt{2}}\frac{\partial u}{\partial y}\right)\left(\frac{\partial u}{\partial y}\right)^2\\+\sigma B^2u^2+Q\left(T-T_\infty\right)\end{bmatrix}. \tag{3}$$

The associate limiting conditions are:

$$\left.\begin{array}{l}u=U_w\left(x\right),\ v=v_w\left(x\right),\ T=T_w\left(x\right),\ \text{at } y=0,\\u\to 0,\ T\to T_\infty,\ \text{as } y\to\infty\end{array}\right\}. \tag{4}$$

Where u and v are velocity components along x and y-directions, respectively. Γ (> 0) denotes the time constant, ρ_∞ is the ambient density, $Q(x) = Q_0x^{m-1}$ and c_p are the coefficients of the heat source/sink, and specific heat, respectively. $K\left(x\right)=\frac{K_0}{x^{m-1}}$ represents the permeability of the porous medium, q_r stands for heat flux, σ refers to the fluid electrical conductivity, and the velocity of suction/blowing is expressed as $v_w(x) = -v_0x^{(m-1)/2}$.

The heat flux q_r based on Rosseland approximation [51], is expressed as

$$q_r=-\frac{4\sigma^*}{3k^*}\frac{\partial T^4}{\partial y}. \tag{5}$$

Consequently, Eq. (3) can be reformulated as follows:

$$u\frac{\partial T}{\partial x}+v\frac{\partial T}{\partial y}=\frac{1}{\rho_\infty c_p}\begin{bmatrix}\frac{\partial}{\partial y}\left(k\left(T\right)\frac{\partial T}{\partial y}\right)+\mu\left(T\right)\left(1+\frac{\Gamma}{\sqrt{2}}\frac{\partial u}{\partial y}\right)\left(\frac{\partial u}{\partial y}\right)^2\\+\sigma B^2u^2+Q\left(T-T_\infty\right)\\+\frac{16\sigma^*}{3k^*}\left(3T^2\left(\frac{\partial T}{\partial y}\right)^2+T^3\frac{\partial^2T}{\partial y^2}\right)\end{bmatrix}. \tag{6}$$

2.4 Similarity transformations

The following similarity transformations are employed to convert the governing PDEs into ODEs, which simplifies the mathematical analysis and enables numerical computation:

$$\begin{array}{l}\eta=\sqrt{\frac{ax^{m-1}}{\upsilon_\infty}}y,\ u=\frac{\partial\psi}{\partial y},\ v=-\frac{\partial\psi}{\partial x},\ \theta\left(\eta\right)=\frac{T-T_\infty}{T_w-T_\infty},\\\psi\left(x\right)=\frac{x}{y}\eta\upsilon_\infty f\left(\eta\right),\ T=T_\infty\left[1+\left(\theta_w-1\right)\theta\left(\eta\right)\right]\end{array} \tag{7}$$

where θ_w stand for temperature ratio aspect.

Substituting Eq. (7) into Eqs. (2), (4), and (6):

$$\begin{array}{l}e^{-\zeta\theta}\left(1+Wf''\right)f'''-\zeta e^{-\zeta\theta}\theta'f''\left(1+\frac{W}{2}f''\right)\\+\left(\frac{m+1}{2}\right)ff''-mf'^2-e^{-\zeta\theta}K_1f'-Mf'=0,\end{array} \tag{8}$$

$$\begin{array}{l}\epsilon\theta'^2+\left(1+\epsilon\theta\right)\theta''\\+\frac{4}{3}\mathrm{N}\begin{bmatrix}\left(1+\left(\theta_w-1\right)\theta\right)^3\theta''\\+3\theta'^2\left(\theta_w-1\right)\left(1+\left(\theta_w-1\right)\theta\right)^2\end{bmatrix}\\+\mathrm{Pr}\begin{bmatrix}\left(\frac{m+1}{2}\right)f\theta'+\mathrm{EcM}f'^2+\mathrm{Q}^*\theta\\+\mathrm{Ec}\left(1+\frac{\mathrm{W}}{2}f''\right)f''^2e^{-\zeta\theta}\end{bmatrix}=0,\end{array} \tag{9}$$

the associated constraints:

$$\text{at } \eta=0;\ f=S,\ f'=1,\ \theta=1 \tag{10}$$

$$\text{as } \eta\to\infty;\ f'\to 0,\ \theta\to 0. \tag{11}$$

2.5 Dimensionless parameters

Dimensionless parameters are:

- $\mathrm{W}=\left(\frac{\sqrt{2}a^{\frac{3}{2}}x^{\frac{3m-1}{2}}}{\sqrt{\nu_\infty}}\right)\Gamma$ (Williamson parameter)
- $\mathrm{Ec}=\frac{U_w^2}{c_p\left(T_w-T_\infty\right)}$ (Eckert number)
- $\mathrm{K_1}=\frac{\nu_\infty}{aK_0}$ (Porosity parameter)
- $\mathrm{Pr}=\frac{\mu_\infty c_p}{k_\infty}$ (Prandtl number)
- $\mathrm{M}=\frac{\sigma {B_0}^2}{a\rho_\infty}$ (Magnetic parameter)
- $\mathrm{N}=\frac{4\sigma^*T_\infty^3}{k_\infty k^*}$ (Radiation number)
- $\mathrm{S}=\frac{\nu_0}{\sqrt{a\nu_\infty}}$ (Suction (> 0)/blowing (< 0) parameter)
- $\mathrm{Q}^*=\frac{Q_0}{a\rho_\infty c_p}$ (Heat source/sink parameter).

Here, we observe that the parameter W vary with x. To resolve this issue, we set $m = 1/3$. Consequently, they took the following form: $\mathrm{W} = \dfrac{\sqrt{2}a^{\frac{3}{2}}\Gamma}{\sqrt{\nu_\infty}}$.

2.6 Physical quantities

Now, we will analyze the assessment of complex physical quantities, specifically the Nusselt number ($\mathrm{Nu_x}$) and the friction factor (C_{f_x}), which are crucial for understanding heat transfer and flow characteristics, respectively. Their specific formulations are as follows:

$$\mathrm{Nu_x} = \frac{xq_w}{k_\infty\left(T_w - T_\infty\right)} \tag{12}$$

$$C_{f_x} = \frac{\tau_w}{\rho_\infty U_w^2}, \tag{13}$$

in which

$$q_w = \left[-k\left(T\right)\left(\frac{\partial T}{\partial y}\right) + q_r\right]_{y=0} \tag{14}$$

$$\tau_w = \left[\mu\left(T\right)\left(1+\frac{\Gamma}{\sqrt{2}}\frac{\partial u}{\partial y}\right)\left(\frac{\partial u}{\partial y}\right)\right]_{y=0}. \tag{15}$$

Substituting Eq. (7) into Eq. (12) and Eq. (13) yields:

$$\mathrm{Nu_x} = -\mathrm{Re_x}^{\frac{1}{2}}\left(1+\frac{4}{3}\mathrm{N}(\theta_w)^3 + \epsilon\right)\theta'(0) \tag{16}$$

$$C_{f_x} = \mathrm{Re_x}^{-\frac{1}{2}}\left(1+\frac{\mathrm{W}}{2}f''(0)\right)f''(0)e^{-\zeta}, \tag{17}$$

where $\mathrm{Re_x} = \dfrac{xU_w}{\nu_\infty}$ is the Reynolds number.

3 Numerical methodology

The non-linear system of ODEs presented in Eqs. (8) and (9), along with the limiting conditions in Eqs. (10) and (11), proves to be difficult to solve using a precise method. In this article, the 4th-order Runge-Kutta technique with a shooting approach has been employed in MATLAB [52] to obtain solutions for the aforementioned model. First, using a first-order process (Fig. 2), we convert the set of non-linear ODEs given in Eqs. (8) and (9) into an IVP, taking into account the limiting terms in Eqs. (10) and (11).

$$f = f_1,\ f' = f_2,\ f'' = f_3,\ \theta = f_4,\ \theta' = f_5$$

$$f_3' = \left(\frac{e^{\zeta f_4}}{1+\mathrm{W}f_3}\right)\left[\begin{array}{l}\zeta e^{-\zeta f_4}f_3 f_5\left(1+\dfrac{\mathrm{W}}{2}f_3\right) - \left(\dfrac{m+1}{2}\right)f_1 f_3 \\ +mf_2^2 + e^{-\zeta f_4}\mathrm{K}_1 f_2 + \mathrm{M}f_2\end{array}\right] \tag{18}$$

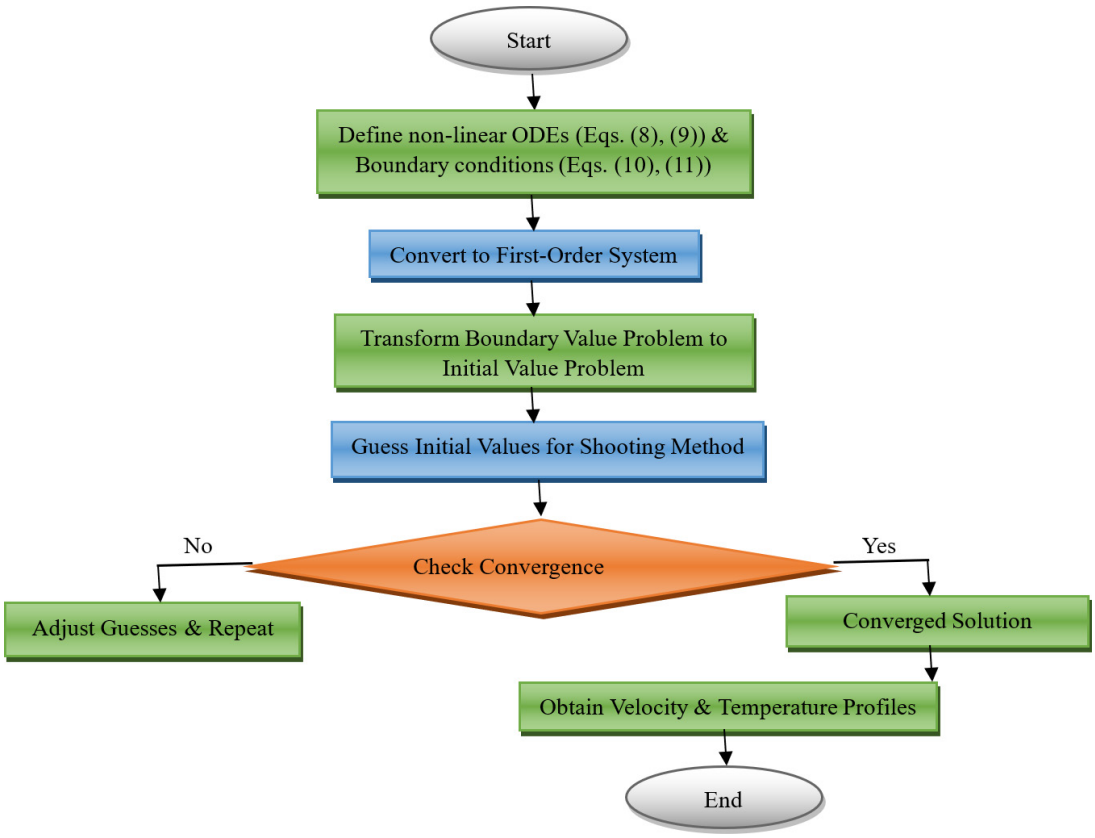


Fig. 2 Numerical solution flowchart

$$f_5' = \frac{1}{\left\{1+\frac{4}{3}\mathrm{N}\left(1+\left(\theta_w-1\right)f_4\right)^3+\epsilon f_4\right\}} \times \left[\begin{array}{l} -\mathrm{Pr}\left[\begin{array}{l}\left(\frac{m+1}{2}\right)f_1f_5+\mathrm{EcM}f_2^2+\mathrm{Q}^*f_4 \\ +\mathrm{Ec}\left(1+\frac{\mathrm{W}}{2}f_3\right)f_3^2e^{-\zeta f_4}\end{array}\right]-\epsilon f_5^2 \\ -4\mathrm{N}f_5^2\left(\theta_w-1\right)\left(1+\left(\theta_w-1\right)f_4\right)^2 \end{array}\right] \quad (19)$$

The associate limiting conditions are:

$$f_1(0)=S,\ f_2(0)=1,\ f_4(0)=1 \quad (20)$$

$$f_2\to 0,\ f_4\to 0 \text{ as } \eta\to\infty. \quad (21)$$

To provide a more accurate estimate of the results, the unknown initial values $f''(0)$ and $\theta'(0)$ are first approximated using suitable initial guesses. These values are then systematically updated through an iterative process until the boundary conditions at infinity are satisfied with a maximal error of 10^{-5} and a step size of $h = 0.01$.

4 Validation of our code

A comparison between our findings and those presented in the previously mentioned literature has been made to evaluate the accuracy of the proposed mathematical technique. By disregarding the factors W, ζ, ϵ, N, Ec, Q^*, K_1, M and S, and setting $m = 1$, our flow model can be reduced to match the conditions studied by Mahmoud and Megahed [47], Wang [53], and Khan and Pop [54]. The findings shown in Table 1 demonstrate strong agreement with these earlier works, thereby validating the accuracy of the numerical method. Thus, the 4th-order Runge-Kutta technique combined with a shooting approach proves to be highly effective and accurate, as evidenced by the comparisons in Table 1.

5 Results and discussion

This segment discusses the influence of several significant factors on velocity and temperature distributions of the Williamson fluid flow over a stretching sheet with the help of tables and sketches. The reference values in the existing article are specified as $W = Ec = \epsilon = 0.2$, $M = Q^* = K_1 = 0.1$, $S = \zeta = 0.5$, $Pr = 2.0$, $N = 0.15$, $\theta_w = 1.5$ and $Re_x = 1$, and have been kept constant throughout the computations.

The ranges of parameters are selected to ensure physical relevance and consistency with previously reported studies. In particular, the Prandtl number is varied within $0.72 \le Pr \le 5.0$, representing fluids such as air and moderately viscous liquids.

The following illustration provides the numerically listed results: velocity $f'(\eta)$ and heat distribution $\theta(\eta)$.

Fig. 3 presents a comparison of the temperature distribution obtained in the present study with the results available in the literature [54] for $Pr = 7.0$, $W = Ec = \epsilon = M = Q^* = K_1 = S = \zeta = N = 0$, and $m = 1$. A close agreement between the two results demonstrates the accuracy and reliability of the present numerical approach.

Fig. 4 (a), (b) presents the variation of the profiles $f'(\eta)$ and $\theta(\eta)$ with respect to ζ, respectively. It is evident that increasing ζ leads to a decrease in the flow amplitude $f'(\eta)$ due to higher viscous resistance (Fig. 4 (a)). In contrast, the temperature profile shows an increasing trend with ζ as a result of enhanced energy dissipation within the fluid (Fig. 4 (b)).

Figs. 5 (a), (b) illustrates the role of the Williamson parameter W on the dimensionless profiles $f'(\eta)$ and $\theta(\eta)$, respectively. An increase in W weakens the velocity field due to the enhanced elastic nature of the fluid, which opposes the motion. Conversely, the temperature rises as the fluid motion becomes restricted, allowing heat to accumulate within the boundary layer.

Fig. 6 (a) illustrates the variation of the velocity $f'(\eta)$ with the magnetic parameter M. An increase in M decreases the profile $f'(\eta)$ due to the action of the Lorentz force, which opposes the fluid motion. Conversely, Fig. 6 (b) shows that the heat profile $\theta(\eta)$ increases with M, as the presence of the magnetic field enhances thermal energy within the thermal limit layer.

Table 1 Comparison of $Re_x^{\frac{-1}{2}} Nu_x$ with previous outcomes

	$Re_x^{\frac{-1}{2}} Nu_x$			
Pr	Mahmoud and Megahed [47]	Wang [53]	Khan and Pop [54]	Present outcome
0.7	0.4539	0.4539	0.4539	0.45444
2.0	0.9114	0.9114	0.9113	0.91134
7.0	1.8954	1.8954	1.8954	1.89538
20.00	3.3539	3.3539	3.3539	3.35386
70.00	6.4622	6.4622	6.4621	6.46213

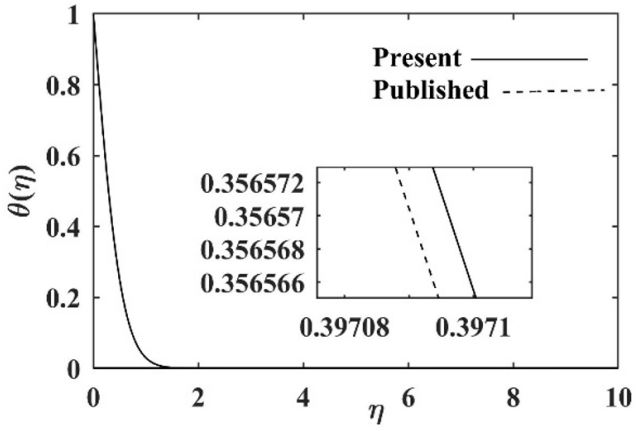


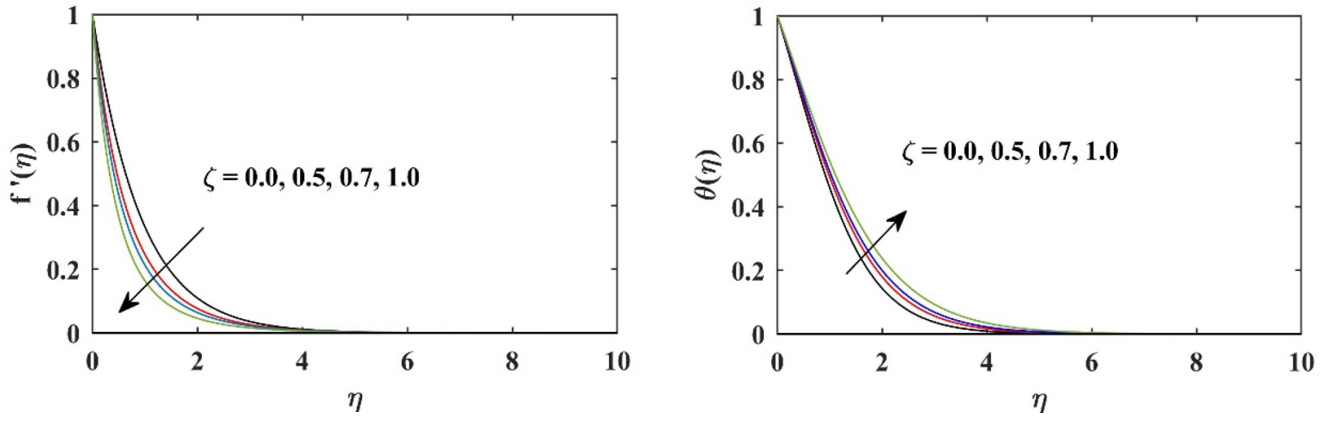
Fig. 3 Comparison of temperature field at Pr = 7.0

Fig. 7 (a), (b) illustrates the effect of S on the velocity $f'(\eta)$ and temperature $\theta(\eta)$ profiles, respectively. It has been found that suction (S > 0) decreases both the flow rate and temperature, whereas blowing (S < 0) enhances them. This behavior is attributed to the modification of the boundary layer thickness, where suction reduces it and blowing increases it. The case of S = 0 signifies a non-porous stretched surface.

Fig. 8 (a), (b) depicts the influence of the parameter K_1 on the profiles $f'(\eta)$ and $\theta(\eta)$, respectively. Notably, increasing K_1 reduces the velocity while enhancing the thermal profile. This behavior is attributed to the increased resistance offered by the porous medium, which restricts fluid motion and promotes heat accumulation within the boundary layer.

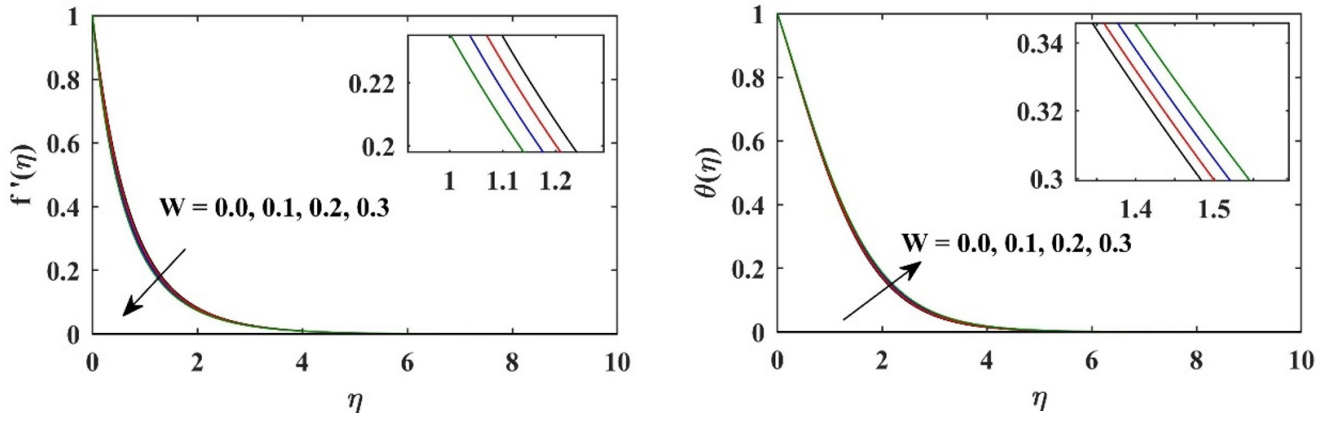
Fig. 9 shows the variation of the profile $\theta(\eta)$ with the Prandtl numbers Pr. It is found that temperature decreases as Pr increases. Physically, a higher Pr indicates a material with greater heat capacity, leading to a thinner thermal limit flake. This behavior is due to the inverse relationship between thermal diffusivity and the Prandtl number, which results in a thinner TBL.

Fig. 10 illustrates the influence of the conductivity parameter ϵ on the profile $\theta(\eta)$. An increase in ϵ enhances the temperature, as higher thermal conductivity promotes heat transfer within the fluid. Consequently, the



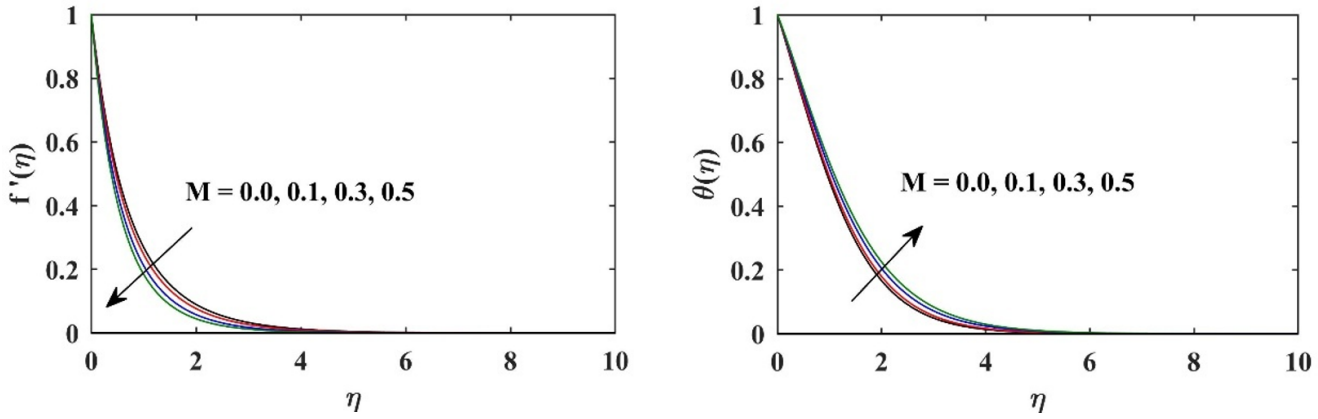
(a) (b)

Fig. 4 Response of (a) velocity and (b) temperature versus η for varied values of ζ



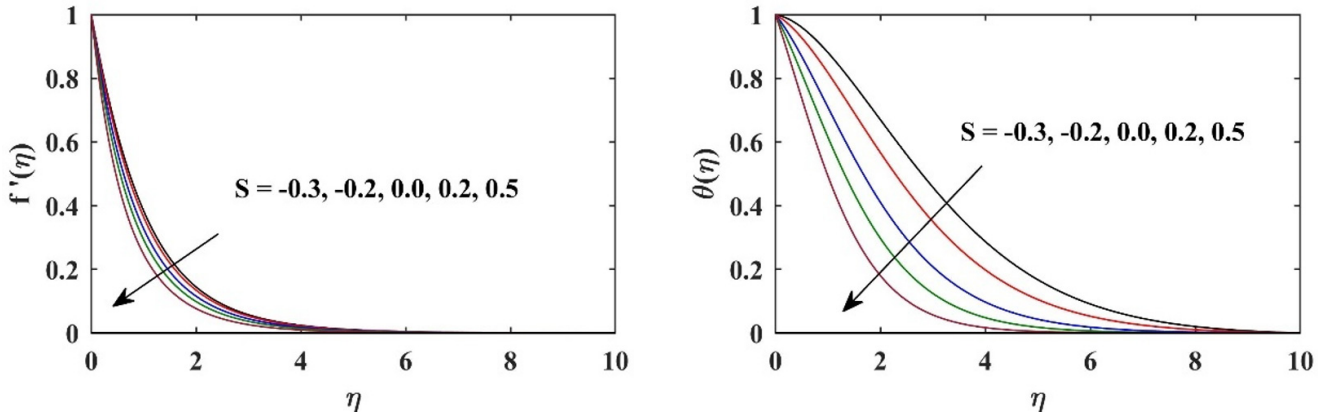
(a) (b)

Fig. 5 Response of (a) velocity and (b) temperature versus η for varied values of W



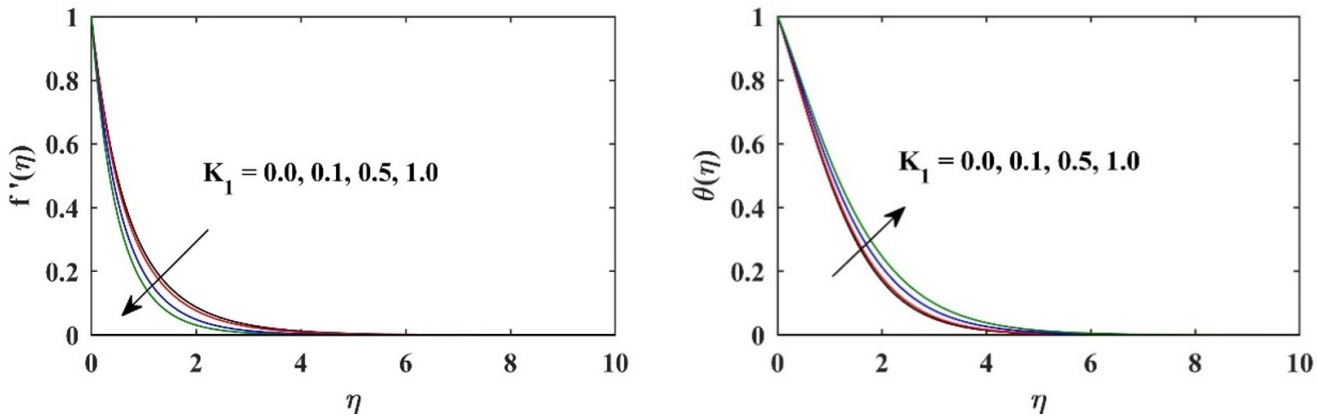
(a) (b)

Fig. 6 Response of (a) velocity and (b) temperature versus η for varied values of M



(a) (b)

Fig. 7 Response of (a) velocity and (b) temperature versus η for varied values of S



(a) (b)

Fig. 8 Response of (a) velocity and (b) temperature versus η for varied values of K_1

thermal boundary layer becomes thicker with increasing ϵ. Additionally, the effect of the radiation parameter N on the dimensionless profile $\theta(\eta)$ is shown in Fig. 11. It is found that $\theta(\eta)$ increases with increasing N, as thermal radiation enhances the energy transport within the fluid.

The effect of the heat source/sink parameter Q^* on $\theta(\eta)$ is depicted in Fig. 12. It is observed that the temperature increases for $Q^* > 0$ (source parameter) and decreases for $Q^* < 0$ (sink parameter). This behavior is attributed to the additional heat supplied to or removed from the fluid,

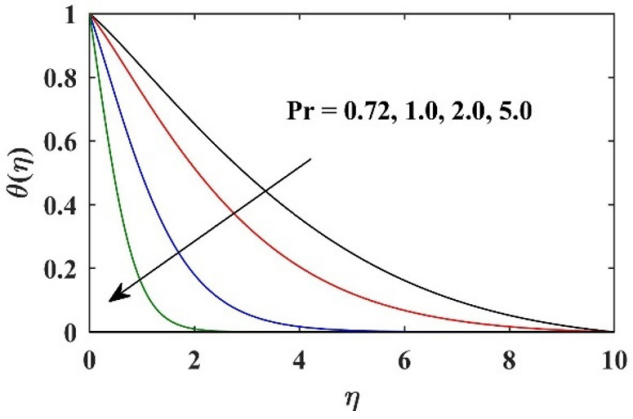


Fig. 9 Response of temperature versus η for varied values of Pr

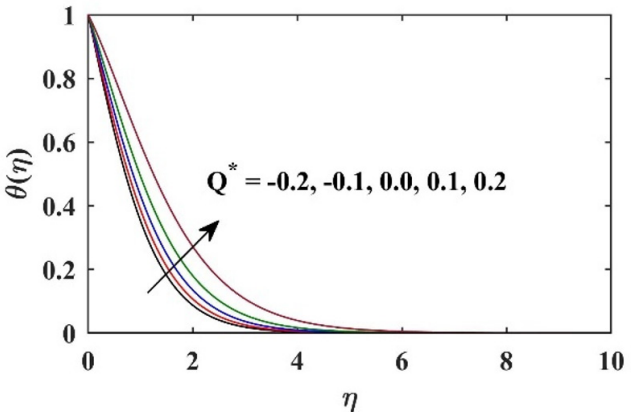


Fig. 12 Response of temperature versus η for varied values of Q^*

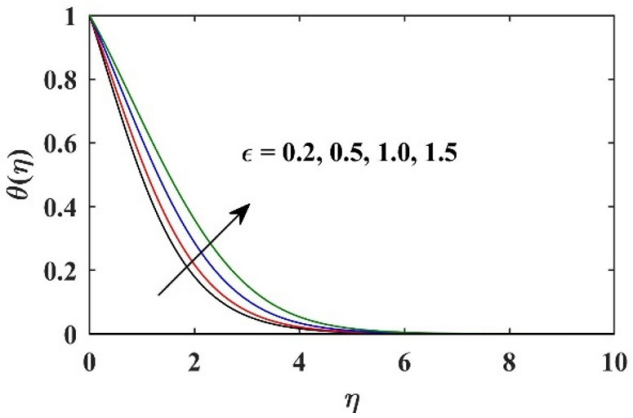


Fig. 10 Response of temperature versus η for varied values of ϵ

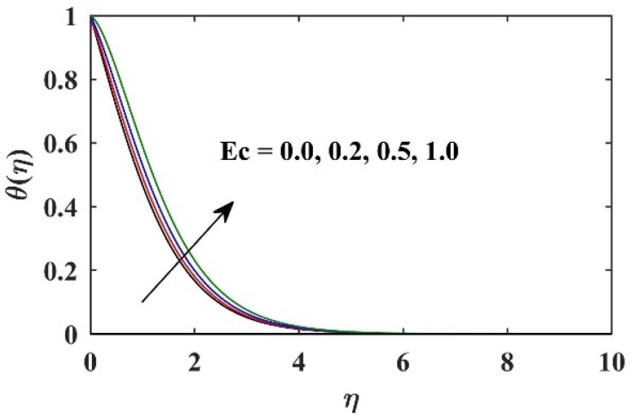


Fig. 13 Response of temperature versus η for varied values of Ec

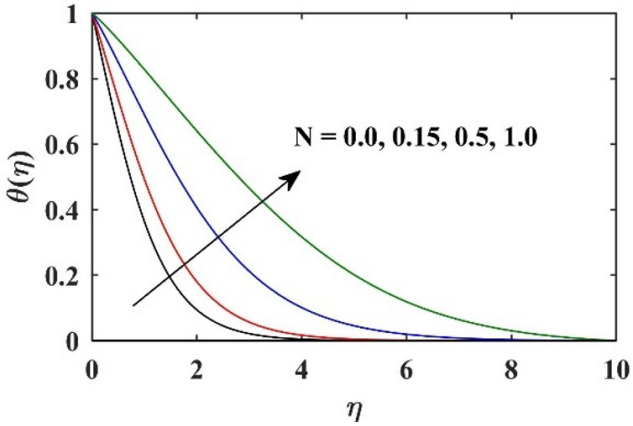


Fig. 11 Response of temperature versus η for varied values of N

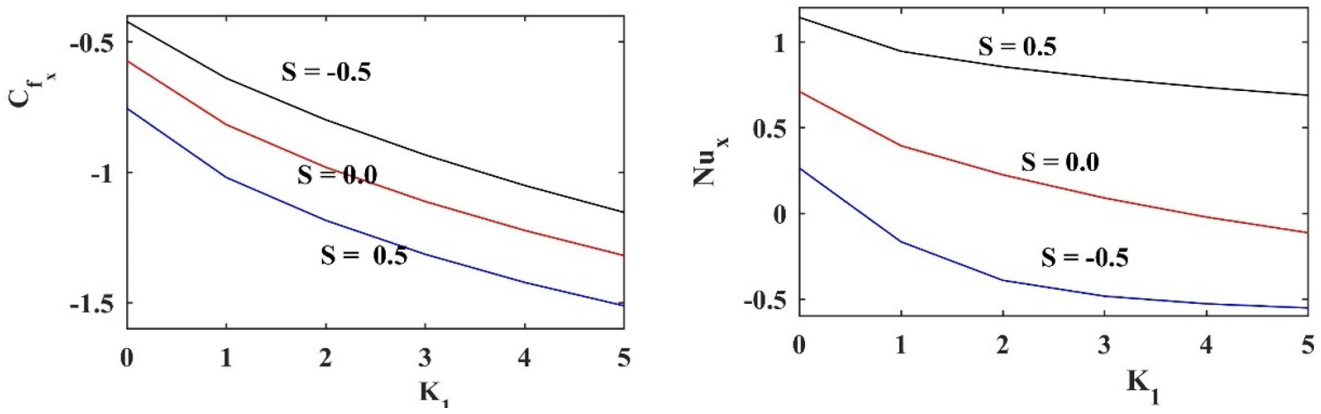
which directly influences the thermal field. Additionally, an increase in $Q^* > 0$ reduces the heat transfer rate, while $Q^* < 0$ enhances it.

Fig. 13 illustrates the variation of the profile $\theta(\eta)$ with the Eckert number Ec. It is observed that the temperature increases with increasing Ec. Physically, when a fluid is influenced by viscous forces, internal energy is generated through the dissipation process, resulting in an enhancement in $\theta(\eta)$.

The evaluation of C_{f_x} and Nu_x against K_1 for different values of S is shown in Fig. 14 (a), (b), respectively. It is observed that C_{f_x} decreases with increasing both parameters, while Nu_x enhances with higher S and decreases with increasing K_1.

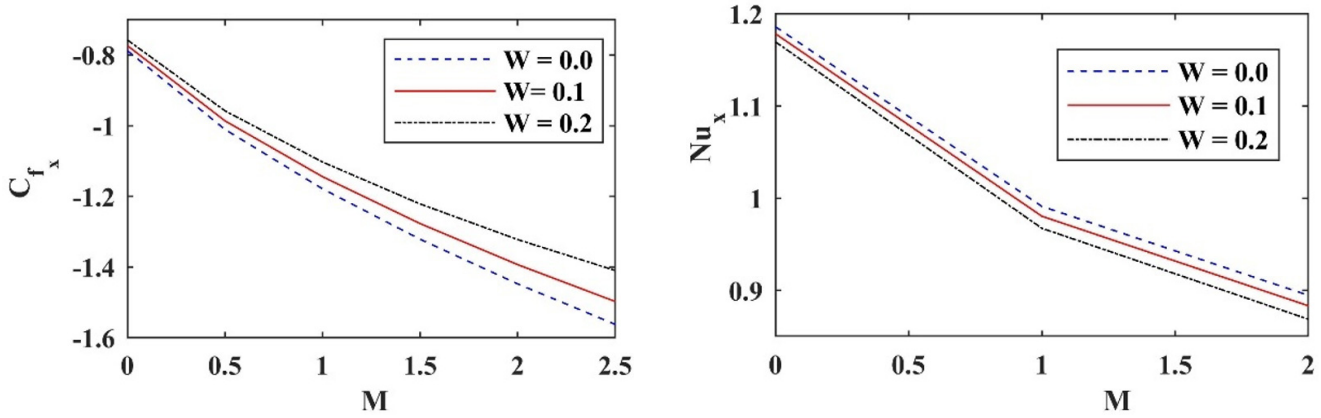
Moreover, Fig. 15 (a), (b) illustrates the behavior of C_{f_x} and Nu_x against M for W = 0.0, 0.1, and 0.2. These profiles reveal that C_{f_x} detracts as M increases and grows as W increases, while Nu_x decreases with increasing both factors.

To comprehensively examine the influence of various governing factors on the dimensionless quantities C_{f_x} and Nu_x, their values have been calculated numerically and presented in tabular form. Table 2 shows the response of C_{f_x} and Nu_x to different governing parameters. It is found that C_{f_x} decreases with increasing values of K_1, S, and Pr, while it increases with rising values of ζ, W, N, ϵ, Ec, and Q^*. Additionally, Table 2 indicates that Nu_x decreases as ζ, W, K_1, ϵ, Ec, and Q^* increase, but it increases with higher values of S, Pr, and N.



(a) (b)

Fig. 14 Response of (a) C_{f_x} and (b) Nu_x against S and K_1



(a) (b)

Fig. 15 Response of (a) C_{f_x} and (b) Nu_x against M and W

6 Conclusions

To highlight the intricacies of heat and mass transmission, an exhaustive explication is provided within the scope of this work. In the current study, the roles of heat sink/source, Joule heating, and dissipation on the radiative MHD flow of Williamson fluid with variable conductivity and viscosity via a non-linear stretching sheet have been evaluated mathematically. The mathematical model has been solved utilizing a fully embedded 4th-order Runge-Kutta method. The numerical results are presented in figures, and following a comprehensive analysis of this intricate physical model, the article draws several explicit conclusions, which are listed below:

- An increase in the parameter S resulted in a decrease in the dimensionless profiles $f'(\eta)$ and $\theta(\eta)$.
- A rise in the parameters ζ, K_1, and M caused a decline in the flow rate.
- The Williamson fluid leads to a rise in temperature $\theta(\eta)$, while it has an inverse impact on the flow rate.
- The heat generation factor Q^* (> 0) increases the temperature, while the absorption factor Q^* (< 0) decreases it.
- An increase in the parameters ζ, ϵ, N, Ec, K_1, and M resulted in an enhancement of temperature, while the effect of Pr was the opposite.
- The local Nusselt number decreased with increasing porosity, heat generation, Williamson, and viscosity parameters, but increased with higher values of the radiation and suction parameters.
- The skin friction factor increased with higher values of the radiation, Williamson, viscosity, and conductivity parameters, and decreased with increasing porosity, Prandtl number, and suction.

Acknowledgment

The writers thank the Ministry of Science & Technology, Government of India, for the CSIR-HRDG Ph.D. grant (09/149(0740)/2019-EMR-I).

Table 2 Computation of C_{f_x} and Nu_x for assorted parameters

ζ	W	K_1	S	Pr	ϵ	N	Ec	Q^*	C_{f_x}	Nu_x
0.0	0.2	0.1	0.5	2.0	0.2	0.15	0.2	0.1	−0.969701	0.991401
0.5	-	-	-	-	-	-	-	-	−0.806509	0.918394
1.0	-	-	-	-	-	-	-	-	−0.666375	0.813375
0.5	0.0	-	-	-	-	-	-	-	−0.840924	0.940350
-	0.2	-	-	-	-	-	-	-	−0.806509	0.918394
-	0.3	-	-	-	-	-	-	-	−0.784991	0.903581
-	0.2	0.0	-	-	-	-	-	-	−0.706891	0.946669
-	-	0.5	-	-	-	-	-	-	−0.807453	0.825938
-	-	1.0	-	-	-	-	-	-	−0.876802	0.736731
-	-	0.1	−0.2	-	-	-	-	-	−0.504906	0.171356
-	-	-	0.0	-	-	-	-	-	−0.566727	0.388406
-	-	-	0.2	-	-	-	-	-	−0.631167	0.599044
-	-	-	0.5	0.72	-	-	-	-	−0.714683	0.258996
-	-	-	-	1.0	-	-	-	-	−0.718378	0.402788
-	-	-	-	5.0	-	-	-	-	−0.752970	2.098669
-	-	-	-	2.0	0.5	-	-	-	−0.803074	0.916719
-	-	-	-	-	1.0	-	-	-	−0.798517	0.907887
-	-	-	-	-	1.5	-	-	-	−0.795039	0.891762
-	-	-	-	-	0.2	0.0	-	-	−0.816636	0.854372
-	-	-	-	-	-	0.15	-	-	−0.806509	0.918394
-	-	-	-	-	-	0.5	-	-	−0.793861	0.925635
-	-	-	-	-	-	0.15	0.0	-	−0.809188	1.103250
-	-	-	-	-	-	-	0.2	-	−0.806509	0.918394
-	-	-	-	-	-	-	0.5	-	−0.802595	0.644250
-	-	-	-	-	-	-	0.2	−0.2	−0.818022	1.455399
-	-	-	-	-	-	-	-	0.0	−0.811283	1.132519
-	-	-	-	-	-	-	-	0.2	−0.799083	0.605438

Nomenclature

u, v – velocity units (m/s)
T_w – wall temperature (K)
T_∞ – ambient temperature (K)
$B(x)$ – variable magnetic field (A/m)
$K(x)$ – porous medium permeability
$Q(x)$ – heat source/sink coefficient
$k(T)$ – variable thermal conductivity (W/(mK))
q_r – radiative heat effluence
q_w – wall heat flux
k_∞ – ambient conductivity
k^* – mean absorption coefficient
Nu_x – Nusselt number
C_{f_x} – local skin-friction coefficient
c_p – specific heat coefficient
K_0 – initial permeability
Q_0, B_0, a – constants
$f'(\eta)$ – dimensionless velocity

Greek symbols

σ – electric conductivity of the fluid (1/Ωm)
Γ – time constant
μ_∞ – ambient viscosity
$\theta(\eta)$ – dimensionless temperature
ρ_∞ – ambient density
η – similarity variable (dimensionless)
ζ – viscosity parameter
$\mu(T)$ – variable viscosity (Ns/m^2)
ψ – stream function
ϵ – conductivity parameter
τ_w – wall stress

List of abbreviations

IVP – Initial value problem
PDEs – Partial differential equations
MHD – Magnetohydrodynamics
ODEs – Ordinary differential equations
2-D – Two-dimensional
TBL – thermal boundary layer

References

[1] Ishak, A., Nazar, R., Pop, I. "Hydromagnetic flow and heat transfer adjacent to a stretching vertical sheet", Heat and Mass Transfer, 44(8), pp. 921–927, 2008. https://doi.org/10.1007/s00231-007-0322-z

[2] Sakiadis, B. C. "Boundary-layer behavior on continuous solid surfaces: I. Boundary-layer equations for two-dimensional and axisymmetric flow", AIChE Journal, 7(1), pp. 26–28, 1961. https://doi.org/10.1002/aic.690070108

[3] Gupta, P. S., Gupta, A. S. "Heat and mass transfer on a stretching sheet with suction or blowing", The Canadian Journal of Chemical Engineering, 55(6), pp. 744–746, 1977. https://doi.org/10.1002/cjce.5450550619

[4] Patel, H. R., Patel, S. D. "Heat and mass transfer in mixed convection MHD micropolar fluid flow due to non-linear stretched sheet in porous medium with non-uniform heat generation and absorption", Waves in Random and Complex Media, 35(2), pp. 2551–2581, 2025. https://doi.org/10.1080/17455030.2022.2044542

[5] Choudhary, P., Loganathan, K., Jat, K., Arunachalam, K. P., Eswaramoorthi, S. "Thermal and velocity slip impacts on MHD tetra-hybrid nanofluids flow over a porous stretching surface", Discover Applied Sciences, 7(7), 720, 2025. https://doi.org/10.1007/s42452-025-07359-6

[6] Jat, K., Sharma, K., Choudhary, P., Soni, P. "Entropy generation analysis of couple stress Casson fluid flow through non-permeable stretching channel", The European Physical Journal Special Topics, 2025. https://doi.org/10.1140/epjs/s11734-025-01525-y

[7] Espinal, L. "Porosity and its measurement", In: Kaufmann, E. N. (ed.) Characterization of Materials, John Wiley & Sons, 2012, pp. 1–10. ISBN 9780471268826 https://doi.org/10.1002/0471266965.com129

[8] Hoath, S. D. "Fundamentals of Inkjet Printing: The Science of Inkjet and Droplets", Wiley-VCH Verlag, 2016. ISBN 9783527337859 https://doi.org/10.1002/9783527684724

[9] Martinez, M. J., McTigue, D. F. "Modelling in nuclear waste isolation: Approximate solutions for flow in unsaturated porous media", In: Environmental Studies, Minneapolis, MN, USA, 1996, pp. 275–289. ISBN 978-1-4613-8494-6 https://doi.org/10.1007/978-1-4613-8492-2_13

[10] Jalili, P., Azar, A. A., Jalili, B., Ganji, D. D. "Study of nonlinear radiative heat transfer with magnetic field for non-Newtonian Casson fluid flow in a porous medium", Results in Physics, 48, 106371, 2023. https://doi.org/10.1016/j.rinp.2023.106371

[11] Hajool, S. S., Harfash, A. J. "Magnetohydrodynamic instability of fluid flow in a bidisperse porous medium", Journal of Engineering Mathematics, 147(1), 10, 2024. https://doi.org/10.1007/s10665-024-10369-9

[12] Sun, D. "Microscale study on dynamics of particles in slurry filtrated through porous media", Computational Particle Mechanics, 11(2), pp. 745–755, 2024. https://doi.org/10.1007/s40571-023-00650-6

[13] Kumar, R., Mehta, R., Bhatnagar, A., Ozsahin, I., Uzun, B., Almohsen, B., Ahmad, H. "Numerical study of Williamson fluid flow over a stretching sheet with Newtonian heating embedded in a porous medium in presence of thermal radiation and heat source/sink", Journal of Nonlinear Mathematical Physics, 32(1), 4, 2025. https://doi.org/10.1007/s44198-024-00258-1

[14] Choudhary, P., Loganathan, K., Jat, K., Sharma, K., Eswaramoorthi, S. "Shape factor analysis of water and aluminium oxide nanoparticles in a porous medium with slip effects", Chemical Physics Impact, 10, 100882, 2025. https://doi.org/10.1016/j.chphi.2025.100882

[15] Suneetha, S., Subbarayudu, K., Reddy, P. B. A. "Hybrid nanofluids development and benefits: A comprehensive review", Journal of Thermal Engineering, 8(3), pp. 445–455, 2022. https://doi.org/10.18186/thermal.1117455

[16] Alfvén, H. "Existence of Electromagnetic-Hydrodynamic Waves", Nature, 150(3805), pp. 405–406, 1942. https://doi.org/10.1038/150405d0

[17] Kolesnichenko, A. V. "Thermodynamic Construction of the MHD Model of Turbulence of Electroconductive Fluid Medium", Solar System Research, 57(7), pp. 706–726, 2023. https://doi.org/10.1134/S0038094623070055

[18] Sharma, S., Goyal, M., Dadheech, A. "Melting, Soret and Dufour effect on MHD Casson fluid flow over a stretching sheet with slip conditions", Journal of Engineering Mathematics, 146(1), 18, 2024. https://doi.org/10.1007/s10665-024-10364-0

[19] Tanwar, M., Mehta, A., Chaurasiya, V. K., Mehta, R. "Computational study of magnetohydrodynamics Williamson fluid flow over stretching surface with Soret and Dufour effects using machine learning", Physics of Fluids, 37(8), 081902, 2025. https://doi.org/10.1063/5.0278881

[20] Mukhopadhyay, S., Vajravelu, K. "Effects of transpiration and internal heat Generation/Absorption on the unsteady flow of a Maxwell fluid at a stretching surface", Journal of Applied Mechanics, 79(4), 044508, 2012. https://doi.org/10.1115/1.4006260

[21] Jyothi, B., Kudenatti, R. B. "Adequate viscosity-induced porous boundary layer flow and heat transfer over a permeable wedge", Journal of Engineering Mathematics, 145(1), 18, 2024. https://doi.org/10.1007/s10665-024-10348-0

[22] Jangid, S., Mehta, R., Bhatnagar, A., Alraddadi, I., Alotaibi, M. F., Ahmad, H. "Heat and mass transfer of hydromagnetic Williamson nanofluid flow study over an exponentially stretched surface with suction/injection, buoyancy, radiation and chemical reaction impacts", Case Studies in Thermal Engineering 59, 104278, 2024. https://doi.org/10.1016/j.csite.2024.104278

[23] Nadeem, S., Hussain, S. T., Lee, C. "Flow of a Williamson fluid over a stretching sheet", Brazilian Journal of Chemical Engineering, 30(3), pp. 619–625, 2013.
https://doi.org/10.1590/s0104-66322013000300019

[24] Williamson, R. V. "The flow of pseudoplastic materials", Industrial and Engineering Chemistry, 21(11), pp. 1108–1111, 1929.
https://doi.org/10.1021/ie50239a035

[25] Saleem, M., Hussain, M. "Impression of nonlinear radiation and Stefan blowing on the magneto cross nano-Williamson fluid above exponentially stretching sheet", Results in Engineering, 17, 100864, 2023.
https://doi.org/10.1016/j.rineng.2022.100864

[26] Zafar, S. S., Zaib, A., Lone, S. A., Mahnashi, A. M., Hamali, W., Saeed, A. "Radiative heat in a Williamson fluid flow through a lubricated surface containing swimming microorganism", Journal of Thermal Analysis and Calorimetry, 150(4), pp. 2633–2650, 2025.
https://doi.org/10.1007/s10973-023-12861-3

[27] Jain, R., Mehta, R., Bhatnagar, A., Ahmad, H., Khan, Z. A., Ismail, G. M. "Numerical study of heat and mass transfer of Williamson hybrid nanofluid (CuO/CNT's-water) past a permeable stretching/shrinking surface with mixed convective boundary condition", Case Studies in Thermal Engineering, 59, 104313, 2024.
https://doi.org/10.1016/j.csite.2024.104313

[28] Choudhary, S., Mehta, R., Mehta, T. "Numerical study of MHD Williamson hybrid nanofluid flow over incessantly moving thin needle in presence of Soret & Dufour effect", Partial Differential Equations in Applied Mathematics, 15, 101294, 2025.
https://doi.org/10.1016/j.padiff.2025.101294

[29] Brinkman, H. C. "Heat effects in capillary flow I", Applied Scientific Research, 2(1), pp. 120–124, 1951.
https://doi.org/10.1007/bf00411976

[30] Weltmann, R. N., Kuhns, P. W. "Effect of shear temperature on viscosity in a rotational viscometer measurement", Journal of Colloid Science, 7(3), pp. 218–226, 1952.
https://doi.org/10.1016/0095-8522(52)90067-6

[31] Gosty, V., Srinivas, G., Babu, B. S., Goud, B. S., Hendy, A. S., Ali, M. R. "Influence of variable viscosity and slip-on heat and mass transfer of immiscible fluids in a vertical channel", Case Studies in Thermal Engineering, 58, 104368, 2024.
https://doi.org/10.1016/j.csite.2024.104368

[32] Imtiaz, M., Ijaz Khan, M., Akermi, M., Hejazi, H. A. "Understanding the impact of magnetic dipole and variable viscosity on nanofluid flow characteristics over a stretching surface", Journal of Magnetism and Magnetic Materials, 589, 171613, 2024.
https://doi.org/10.1016/j.jmmm.2023.171613

[33] Ou, J. W., Cheng, K. C. "Viscous dissipation effects on thermal entrance region heat transfer in pipes with uniform wall heat flux", Applied Scientific Research, 28(1), pp. 289–301, 1973.
https://doi.org/10.1007/bf00413074

[34] Parveen, N., Alim, M. A. "Joule heating effect on magnetohydrodynamic natural convection flow along a vertical wavy surface", Journal of Naval Architecture and Marine Engineering, 9(1), pp. 11–24, 2012.
https://doi.org/10.3329/jname.v9i1.5954

[35] Sadia, H., Mustafa, M., Farooq, M. A. "Numerical and series solutions for Von-Kármán flow of viscoelastic fluid inspired by viscous dissipation and Joule heating effects", Alexandria Engineering Journal, 75, pp. 181–190, 2023.
https://doi.org/10.1016/j.aej.2023.05.075

[36] Ahmed, S. E., Arafa, A. M., Hussein, S. A. "Viscous dissipation and Joule heating in case of variable electrical conductivity Carreau–Yasuda nanofluid flow in a complex wavy asymmetric channel through porous media", Modern Physics Letters B, 38(36), 2450369, 2024.
https://doi.org/10.1142/s021798492450369x

[37] Chamkha, A. J., Issa, C. "Effects of heat generation/absorption and thermophoresis on hydromagnetic flow with heat and mass transfer over a flat surface", International Journal of Numerical Methods for Heat & Fluid Flow, 10(4), pp. 432–449, 2000.
https://doi.org/10.1108/09615530010327404

[38] Barman, D. "Effect of internal heat source on stability analysis of a highly permeable vertical porous channel filled with nanofluid", Journal of Engineering Mathematics, 140(1), 11, 2023.
https://doi.org/10.1007/s10665-023-10275-6

[39] Islam, T., Alam, M. N., Niazai, S., Khan, I., Fayz-Al-Asad, M., Alqahtani, S. "Heat generation/absorption effect on natural convective heat transfer in a wavy triangular cavity filled with nanofluid", Scientific Reports, 13(1), 21171, 2023.
https://doi.org/10.1038/s41598-023-48704-2

[40] Subray, P. V. A., Hanumagowda, B. N., Varma, S. V. K., Chouhan, J. S., Yogeesha, K. M., Madhu, J., Kumar, R. N. "Impact of electromagnetic field on three-phase flow of dissipative and radiative Casson hybrid nanofluid with internal heat generation/absorption", Pramana - Journal of Physics, 98(2), 38, 2024.
https://doi.org/10.1007/s12043-023-02724-9

[41] Mahmoud, M. A. A. "Thermal radiation effects on MHD flow of a micropolar fluid over a stretching surface with variable thermal conductivity", Physica A: Statistical Mechanics and its Applications, 375(2), pp. 401–410, 2007.
https://doi.org/10.1016/j.physa.2006.09.010

[42] Alrihieli, H. "Thermal and concentration slip impact on the dissipative Casson–Maxwell nanofluid flow due to a stretching sheet with heat generation and thermal radiation", The European Physical Journal Plus, 138(10), 916, 2023.
https://doi.org/10.1140/epjp/s13360-023-04525-w

[43] Prakash, J., Tripathi, D., Kumar Tiwari, A., Kumar Pandey, A. "Melting heat transfer and irreversibility analysis in Darcy-Forchheimer flow of Casson fluid modulated by EMHD over cone and wedge surfaces", Thermal Science and Engineering Progress, 52, 102680, 2024.
https://doi.org/10.1016/j.tsep.2024.102680

[44] Al-Shammari, H., Ullah, Z., Mahrous, Y. M., Aldhabani, M. S., Said, M. A., Al Arni, S., Faqihi, A. A., Ben Khedher, N. "Arrhenius activation energy and thermal radiation effects on oscillatory heat-mass transfer of Darcy Forchheimer nanofluid along heat generating cone", Case Studies in Thermal Engineering, 57, 104294, 2024.
https://doi.org/10.1016/j.csite.2024.104294

[45] Jat, K., Sharma, K., Choudhary, P., Soni, P. "Bioconvection of a radiating and reacting nanofluid flow past a nonlinear stretchable permeable sheet in a porous medium", Journal of Biological Physics, 51(1), 8, 2025.
https://doi.org/10.1007/s10867-025-09669-7

[46] Megahed, A. M. "Williamson fluid flow due to a nonlinearly stretching sheet with viscous dissipation and thermal radiation", Journal of the Egyptian Mathematical Society, 27, 12, 2019.
https://doi.org/10.1186/s42787-019-0016-y

[47] Mahmoud, M. A. A., Megahed, A. M. "MHD flow and heat transfer in a non-Newtonian liquid film over an unsteady stretching sheet with variable fluid properties", Canadian Journal of Physics, 87(10), pp. 1065–1071, 2009.
https://doi.org/10.1139/p09-066

[48] Krishna, M. V., Chamkha, A. J. "Hall effects on MHD squeezing flow of a water-based nanofluid between two parallel disks", Journal of Porous Media, 22(2), pp. 209–223, 2019.
https://doi.org/10.1615/jpormedia.2018028721

[49] Mandal, B., Layek, G. C. "Unsteady MHD mixed convective Casson fluid flow over a flat surface in the presence of slip", International Journal of Modern Physics C, 32(03), 2150038, 2021.
https://doi.org/10.1142/s0129183121500388

[50] Kumar, P., Yadav, R. S., Makinde, O. D. "Numerical study of Williamson fluid flow and heat transfer over a permeable stretching cylinder with the effects of Joule heating and heat generation/absorption", Heat Transfer, 52(4), pp. 3372–3388, 2023.
https://doi.org/10.1002/htj.22832

[51] Brewster, M. Q. "Thermal radiative transfer and properties", John Wiley & Sons, 1992. ISBN 978-0-471-53982-7

[52] The MathWorks, Inc. "MATLAB, (Version R2017b)", [computer program] The MathWorks, Inc., Natick, MA, USA, 2017.

[53] Wang, C. Y. "Liquid film on an unsteady stretching surface", Quarterly of Applied Mathematics, 48(4), pp. 601–610, 1990.
https://doi.org/10.1090/qam/1079908

[54] Khan, W. A., Pop, I. "Boundary-layer flow of a nanofluid past a stretching sheet", International Journal of Heat and Mass Transfer, 53(11–12), pp. 2477–2483, 2010.
https://doi.org/10.1016/j.ijheatmasstransfer.2010.01.032